Validity of the dielectric approximation in describing electron-energy-loss spectra of surface and interface phonons in thin films of ionic crystals

Ph. Lambin, P. Senet, and A. A. Lucas
Institute for Studies in Interface Sciences, Facultés Universitaires Notre Dame de la Paix, Rue de Bruxelles 61, B-5000 Namur, Belgium
(Received 20 March 1991)

The dielectric approximation has proven useful in interpreting experimental data obtained by electron-energy-loss spectroscopy (EELS) in specular geometry at the surface of a large variety of materials, including artificial (multi)layered systems. This approximation can no longer be applied to very thin films as the concept of a bulk dielectric function—the only input required in this approach—breaks down when used for a slab of a few atomic planes. In this paper, a formalism is developed allowing microscopic calculations of the phonon surface response function relevant to specular EELS in the case of thin films of ionic materials. Two test cases are analyzed in some detail: $CaF_2(111)$ isolated films and RbF(001) layers on a thick Ge substrate. EELS spectra are obtained from shell-model, lattice-dynamical calculations for relaxed films and compared with the predictions of the dielectric approximation. It is shown that the dielectric approximation reproduces the essential features of the phonon response when the layer thickness exceeds 20–30 Å. However, even for films having that thickness, small contributions of microscopic surface phonons survive and these may not be negligible. It is shown, in particular, that the S_2 surface microscopic phonon of RbF(001) is responsible for doubling the intensity of the loss structure in the region of the "interface" macroscopic Fuchs-Kliewer phonon predicted by the dielectric approximation in RbF/Ge.

I. INTRODUCTION

The technique of making artificial materials having a layered structure has progressed considerably during the past several decades to the point where such multilayered systems are now produced routinely for (opto)electronic applications.[1] From a fundamental point of view, producing epitaxial growth of a film on various crystalline substrates in well-controlled experimental conditions offers the opportunity to investigate interfacial properties of the coexisting materials. Among these properties, the phonon structure of an interface is of great current interest.[1] High-resolution electron-energy-loss spectroscopy (HREELS) is one of several techniques available today for such investigations. Although primarily a surface-sensitive technique, HREELS in specular geometry provides information about the interfacial region when the thickness of the topmost layer does not exceed the probing depth, typically 10–50 nm in low-energy experiments.[3]

Coulomb interactions between the impinging electrons and macroscopic charge oscillations that develop at the surface of the target are responsible for the so-called dipolar scattering regime that dominates the EELS spectrum in specular geometry.[4] From the theory side, the quantitative understanding of the dipolar-scattering mechanism has been available for a long time.[5,6] Within a purely classical description of the charge oscillations that develop at the surface or interface, it is found that the probability for an electron to be inelastically backscattered by emission of an excitation of frequency ω and wave vector $\mathbf{Q}$ parallel to the surface is proportional to the imaginary part of the so-called surface dielectric response function $g(\mathbf{Q},\omega)$ of the medium.[7,8] The complete expression of the inelastic cross section also involves a kinematic prefactor that only depends on experimental parameters and which presents a sharp maximum at a wave vector $Q \approx \omega/v$, where v is the electron velocity.[5,6] For phonon spectroscopy in low-energy EELS, ω/v is 0.1 nm^{-1} typically, a quantity small compared to the extension of the first Brillouin zone.

For quantitative comparisons with experimental data, the classical theory of EELS must be complemented by a suitable quantum statistical treatment of the surface excitations, which are viewed as quantum-mechanical harmonic oscillators driven by the Coulomb force exerted by the probing electrons.[5,9] In the harmonic approximation, application of the theory for an arbitrary target temperature only demands the 0-K response function $g(\mathbf{Q},\omega)$ of the medium to an external electric field having the form of a plane wave $e^{i\mathbf{Q}\cdot\boldsymbol{\rho}-i\omega t}$ in directions $\boldsymbol{\rho}$ parallel to the surface. Since Q is small, electrostatics is generally sufficient for providing the target response required for applications to near-specular EELS. This approach is known as the dielectric approximation. Expressions of g deduced from electrostatics are available for a large variety of systems, including arbitrary plane-stratified materials.[10] Such expressions, which demand the long-wavelength bulk dielectric functions of the successive layers, are certainly valid at small Q's when the layer thicknesses are large on the atomic scale. By contrast, very thin layers require a microscopic treatment,[11] since the use of a bulk dielectric function for the response of a film composed of a few atomic planes is highly questionable.

Owing to the relation of the surface dielectric response

function g to many physical phenomena,[12] the determination of g from microscopic calculations has been the subject of an already vast theoretical effort.[13] How this problem can be tackled strongly depends upon the kind of material under investigation and the frequency range of interest. In the infrared domain, information about the surface response of phonons to long-wavelength excitations can be gained by evaluating the macroscopic polarization they produce.[14] An advantage of this approach is that the macroscopic polarization is a quantity directly accessible to electronic self-consistent calculations.[15,16] This *ab initio* technique is particularly well adapted to elemental semiconductors, III-V compounds, or *s-p* bonded metals where pseudopotentials and plane-wave expressions make the computation feasible.

The phonon structure of ionic insulators can be accurately described by a standard lattice-dynamical model with parameters fitted to experimental data. In the infrared domain, g can be obtained by solving lattice-dynamical equations in the presence of an external electric field,[17] a point of view that was used in the early 1970s by Jones and Fuchs, who developed a microscopic theory of the reflection and transmission coefficients of a slab using the rigid-ion approximation.[18] The present paper is based on a version of the theory of Jones and Fuchs generalized to a shell model [19] but excluding retardation effects (negligible in low-energy EELS). The central question that is addressed here concerns the minimum layer thickness required to validate the use of the dielectric approximation in the interpretation of EELS for phonon excitations and to assess the importance of microscopic modes for thinner films. The main motivation for this work is the experimental finding that the dielectric approximation fails in describing accurately EELS data for very thin films of CaF_2 on Si(111).[20] Let us immediately note that we are not able to apply our formalism directly to such an overlayer system for reasons that will be made clear in Sec II. Nevertheless, the results of microscopic calculations performed for both CaF_2 *isolated* films and for a simplified model of an insulating overlayer, namely RbF(001)Ge, allow us to present a possible interpretation of the experimental EELS spectra of CaF_2/Si(111).

The paper is organized as follows. In Sec. II, a methodology is developed for treating the interactions of a film with a thick substrate. For the long-wavelength optical excitations of interest in EELS, the substrate is viewed as a continuous dielectric medium, whereas the dynamics of the overlayer is treated using the microscopic approach. This model, fully consistent with electrostatics in the treatment of the substrate response, allows us to focus on layer-thickness effects in the surface dielectric function. How to deduce the surface dielectric function from either electrostatics or the microscopic phonon structure of the film is briefly summarized in Sec. III, technical details being provided in the Appendix. The results of test calculations are illustrated and analyzed in Secs. IV and V. We first consider a self-supported geometry by investigating the response function of isolated CaF_2(111) films. As previously illustrated[17] for NaF(001) slabs described within a rigid-ion approximation (an approach much simpler than the shell model considered here), the case of an isolated film already provides an answer to the question we have raised about the layer thickness. Specific thickness effects for an overlayer geometry will be examined in Sec. V where we investigate the surface response function of RbF(001) films on Ge. Discussion of the results obtained and conclusions are presented in Sec. VI.

II. SLAB DYNAMICS IN THE OVERLAYER GEOMETRY

The surface dielectric response of a film on a thick substrate could in principle be obtained by lattice-dynamics calculations if information were available about the atomic structure and the force constants at the interface between the two materials. As far as macroscopic optical phonons are concerned, the intrinsic difficulty of treating the perturbation brought about by a surface or an interface on the long-range Coulomb fields introduces a further complication that renders Green's-function techniques inadequate in reproducing the long-wavelength Fuchs-Kliewer surface and interface phonons.[21] As another alternative, representing the substrate by a slab of finite thickness would require, in principle, a substrate thickness of the order of the wavelength of the modes of interest (100–500 Å, typically), making the size of the dynamical matrix exceedingly large.

In view of these difficulties and of our desire to characterize properly the long-wavelength optical response of the system, we decided not to treat the substrate at the atomic level but rather consider it as a semi-infinite dielectric medium. In this semimicroscopic model, there is no need for a bulk dielectric function of the film: the surface response of the system is obtained by solving the dynamical equations for the ions of the film, including the interactions with their image charges symmetrically located with respect to the interface and following instantaneously the positions of the source charges. The image approximation is fully consistent with the macroscopic approach that works remarkably well when the overlayer is large enough to validate the use of its bulk dielectric function. This point of view is also the one adopted in treating EELS spectroscopy of isolated molecules absorbed at the surface of a metal.[22,23] In the present problem we have a crystalline film instead of isolated species, with strong interactions between the ions in the overlayer.

Figure 1 illustrates the positions of the ions and their images for a film having the NaCl structure with a (001) interface visualized by the dot-dashed line. The image charges are screened by the factor $\beta=(\epsilon_2-1)/(\epsilon_2+1)$ where ϵ_2 denotes the bulk dielectric function of the substrate, which could in principle be frequency dependent. When we investigate below the static properties of the model, the static dielectric constant $\epsilon_2(0)$ will be used. However, in order to simplify the formulation of the dynamical properties of the film, β will be assumed constant in the frequency interval of the optical modes. This approximation is justified for the case of ionic films on intrinsic silicon or germanium or on a free-electron metallic substrate. Notice that several systems of the kind con-

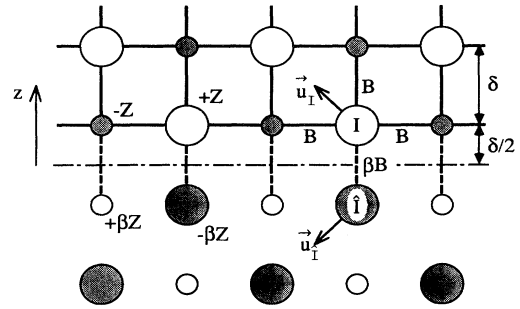

FIG. 1. Static positions of the ions and their images for a film having the NaCl(001) structure on a semi-infinite dielectric substrate. In this model, the interface with the substrate (dot-dashed line) acts as a mirror plane. Short-range interactions between neighboring atoms in the film are schematized by the solid lines ("bonds") in the figure. The dashed lines represent the "broken bonds" at the interface.

sidered below, namely, insulating layers on Si or Ge, have a number of potential applications in semiconductor technology.[24]

Let us first analyze the model displayed in Fig. 1 from a static point of view and consider a *thick* film (ideally a semi-infinite one) on a perfect conductor ($\beta=1$). Assuming that the image plane (the interface) is located $\delta/2$ below the lowest atomic layer of the semi-infinite crystal, where δ is the interplane distance, and ignoring for the moment any atomic relaxation, the static images for the particular geometry of Fig. 1 match, both in charges and in equilibrium position, the charges one would have in the nonterminated crystal. As a consequence of this property of the NaCl(001) interface model, the static Coulomb force on any ion of the film in the presence of their images is exactly zero as it is in the bulk crystal. This would no longer be true for another interface orientation in the NaCl structure nor for, e.g., a CaF_2 lattice with a (111) interface.

On any bulk NaCl lattice site, short-range repulsive interaction forces originating from the neighboring ions also cancel. Restricting for the moment the discussion to first-neighbor anion-cation short-range interactions, the repulsive forces in the bulk crystal all have the same amplitude, generally expressed in terms of a dimensionless negative constant B, the so-called transverse force constant,[25] through the expression $-Be^2/[4\pi\epsilon_0(2r_0)^2]$, where e is the electron charge, ϵ_0 is the permittivity of vacuum, and r_0 is the equilibrium distance. Close to the interface, the short-range interactions on the ion I located at the lowest atomic layer of Fig. 1 will not compensate each other unless one invokes some repulsive forces $\mathbf{F}_S$ with the substrate which exactly restore local equilibrium.

For the case of a dielectric substrate with $\beta<1$, the Coulomb image forces are reduced by the factor β. Similarly, the short-range repulsion force $\mathbf{F}_S$ will be screened by the same factor, taking for the ion I in Fig. 1

$$\mathbf{F}_S(I)=\beta\frac{-Be^2}{4\pi\epsilon_0(2r_0)^2}\hat{\mathbf{e}}_z\ , \tag{2.1}$$

where $\hat{\mathbf{e}}_z$ denotes the unit vector along the z direction normal to the interface and B is the bulk transverse force constant of the film. The total static force on ion I at the interface is now

$$\mathbf{F}(I)=(1-\beta)\alpha'\frac{(Ze)^2}{(4\pi\epsilon_0 r_0^2}\hat{\mathbf{e}}_z+(1-\beta)B\frac{e^2}{4\pi\epsilon_0(2r_0)^2}\hat{\mathbf{e}}_z\ . \tag{2.2}$$

The first term in this expression is the Madelung contribution, equal to the difference between the Coulomb forces set up at site I by all the ions of the film and those originating from the β-screened image in the substrate, α' in Eq. (2.1) being a dimensionless constant that can be computed numerically with high precision and whose value for NaCl(001) is $\alpha'=0.294\,66$. The second term in Eq. (2.2) is the net short-range repulsive force including the substrate contribution [Eq. (2.1)].

The bulk transverse force constant B can be expressed in terms of the bulk Madelung constant α_M of the crystal through the bulk equilibrium condition $B+\frac{2}{3}\alpha_M Z^2=0$, where Z is the absolute ionic charge in units of e. As a result, Eq. (2.2) simplifies to

$$\mathbf{F}(I)=(1-\beta)(\alpha'-\alpha_M/6)\frac{(Ze)^2}{4\pi\epsilon_0 r_0^2}\hat{\mathbf{e}}_z\ . \tag{2.3}$$

This force vanishes identically for $\beta=1$, as already pointed out previously for a perfectly conducting substrate. When β is less than 1, there remains a residual force on the ion I. This force is actually small because α' in the present geometry is very close to $\alpha_M/6=0.291$. Since the prefactor $1-\beta$ in Eq. (2.3) is smaller than 1, the residual force on the ions in contact with the substrate in the present model is always smaller than that one which would exist at a free surface ($\beta=0$). By optimizing the geometry, such small residual static forces close to the interface can be eliminated, following a relaxation procedure usually worked out at a free surface.[26]

The static properties of a *thin* film, for which we are still using the expression [Eq. (2.1)] for the substrate-induced repulsive force, are essentially the same as those derived here above for a *thick* film. Indeed, for instance, α' for a three-layer NaCl(001) slab has already converged up to the sixth decimal place to the value given above for a semi-infinite film. Let us also point out that Eq. (2.3) can be generalized to the case where second-neighbor anion-anion and cation-cation short-range interactions B' and B'' are required by the shell-model parametrization.

Performing lattice-dynamics calculations in the harmonic approximation still demands expressions for the dynamical force constants. The force constants are easy to derive when expressions of the interaction pair potentials are given in terms of separation distances. Besides, relaxing the structure, as mentioned above, also requires expressions of the potentials or the forces. For the Coulomb contributions, the Coulomb potential is available. As for the repulsive ion-ion forces, we explicitly as-

sume the existence of a central, short-range potential $V(r)$ between neighboring ions, restricting again the present discussion to anion-cation first-neighbor pairs. The hypothesis of a central potential is in fact a requisite to establishing the aforementioned relation between the transverse force constant B and the Madelung constant α_M. With this potential $V(r)$ at hand, taken from the bulk three-dimensional crystal, we introduce a short-range repulsive potential with the substrate by considering that ion I at the interface, with instantaneous position $\mathbf{r}_I$, is moving in the additional potential $\frac{1}{2}\beta V(|\mathbf{r}_I-\mathbf{r}_{\hat{I}}|)$ where $r_{\hat{I}}$ is the position of the image of I (Fig. 1). As a justification for this choice, consider small displacements $\mathbf{u}_I$ and $\mathbf{u}_{\hat{I}}=\mathcal{I}\mathbf{u}_I$ of the ion and its image around their equilibrium positions, where $\mathcal{I}$ is the "imaging" diagonal matrix

$$\mathcal{I}=\begin{bmatrix}1&0&0\\0&1&0\\0&0&-1\end{bmatrix} . \tag{2.4}$$

The repulsive potential with the substrate developed to first order in the displacements is then written as $\frac{1}{2}\beta V(r_0)-\mathbf{F}_S(I)\cdot\mathbf{u}_I$, where $\mathbf{F}_S(I)$ is precisely, by construction, the static force introduced in Eq. (2.1), accounting for

$$\left.\frac{dV}{dr}\right|_{r=r_0}=B\frac{e^2}{4\pi\epsilon_0(2r_0)^2} , \tag{2.5}$$

which follows from the definition of the constant B.

It may be argued that one can construct infinitely many potentials $V(r)$ fulfilling the condition (2.5), but the repulsive anion-cation potential taken from the bulk crystal turned out to be the best in reproducing the dispersion curve of the Fuchs-Kliewer interface phonon such as predicted by electrostatics close to the $\bar{\Gamma}$ point. In the absence of any other information, this choice is thus the natural one, remembering that lattice dynamics for macroscopic optical phonons must reproduce electrostatics predictions, at least for reasonably thick films. In so doing, the dynamics of the overlayer can be solved without introducing any new parameters in addition to those available for the bulk crystal and the β screening constant, in keeping with the electrostatics point of view that only demands the bulk dielectric functions of the individual materials.

The dynamical equations for the ions of the film in the present NaCl(001) geometry can now be derived in a simple way. In the expression of the total potential energy U of the film, in addition to the usual terms for a self-supported film, the role of the substrate is taken into account via the following screened contribution:

$$U_S=\tfrac{1}{2}\beta\sum_J\sum_{\hat{I}}V_{J\hat{I}}(|\mathbf{r}_J-\mathbf{r}_{\hat{I}}|) . \tag{2.6}$$

Equation (2.6) implies a sum over all the ions J of the film and their images $\hat{I}$ in the substrate. $V_{J\hat{I}}(r_{J\hat{I}})$ now denotes all the interactions that would exist across the interface between the ions at sites J and $\hat{I}$ in the nonterminated crystal, including both the Coulomb potential $Z_JZ_Ie^2/(4\pi\epsilon_0 r_{J\hat{I}})$ and the repulsive short-range interactions, which need no longer be restricted to the sole first-neighbor pairs. The potential energy [Eq. (2.6)], valid for rigid ions, is easily generalized to deformable ions in a shell-model description.

Within the usual harmonic approximation, developing Eq. (2.6) to second order in the displacements $\mathbf{u}$ and $\mathcal{I}\mathbf{u}$ of the ions and images, the substrate contribution to the equations of motion is readily derived in the following form:

$$-\frac{\partial U_S}{\partial\mathbf{u}_I}=\frac{\beta}{2}\left[\sum_J(\phi_{I\hat{J}}+\mathcal{I}\phi_{J\hat{I}}\mathcal{I})\right]\mathbf{u}_I -\frac{\beta}{2}\sum_J(\phi_{I\hat{J}}\mathcal{I}+\mathcal{I}\phi_{J\hat{I}})\mathbf{u}_J , \tag{2.7}$$

with I and $J=1,\ldots,N$, N being the number of ions in the film. In Eq. (2.7), which represents the dynamical force on the ion I mediated by the dielectric substrate underneath $\phi_{J\hat{I}}$ denotes the force-constant symmetric tensor

$$\phi_{J\hat{I}}=-\left[V''_{J\hat{I}}-\frac{V'_{J\hat{I}}}{r^0_{J\hat{I}}}\right]\frac{\mathbf{r}^0_{J\hat{I}}\mathbf{r}^0_{J\hat{I}}}{r^{0^2}_{J\hat{I}}}-\frac{V'_{J\hat{I}}}{r^0_{J\hat{I}}}E , \tag{2.8}$$

where the first and second derivative V' and V'' of the potentials are evaluated at the equilibrium distances $r^0_{J\hat{I}}$ and E is the unit tensor. The Coulomb force-constant tensors have the property that $\mathcal{I}\phi_{J\hat{I}}\mathcal{I}=\phi_{I\hat{J}}$ and, as a consequence $\mathcal{I}\phi_{J\hat{I}}=\phi_{I\hat{J}}\,\mathcal{I}$. As a final remark, let us point out that the right-hand side of Eq. (2.7), when taking all the displacements equal to a constant vector $\mathbf{u}$ along the z direction, does not reduce to zero because the interface with the massive, undeformable substrate is kept fixed in space. This drawback of the model, which is not suitable for including the elastic properties of the substrate, should not much affect the optical excitations of the supported film.

III. SURFACE DIELECTRIC RESPONSE

The phonon contribution to the surface dielectric response of a film made from a polar crystal can be obtained by solving lattice-dynamics equations in the presence of an external electric potential having the form of a plane wave in directions $\boldsymbol{\rho}$ parallel to the surface and satisfying Laplace's equation outside the sources. In the material region, in particular, the excitation potential takes the form

$$\phi_e=Ae^{Qz}e^{i\mathbf{Q}\cdot\boldsymbol{\rho}-i\omega t} , \quad z<0 \tag{3.1}$$

$z=0$ being the geometrical surface plane. Due to the excitation electric field, forced oscillations of the ions around their equilibrium positions take place, inducing an electric field whose expression in the vacuum region ($z>0$) above the film and far away from its free surface derives from the potential

$$\phi_{\text{ind}}=-g(\mathbf{Q},\omega)Ae^{-Qz}e^{i\mathbf{Q}\cdot\boldsymbol{\rho}-i\omega t} , \quad z\gg\delta , \tag{3.2}$$

where δ is a typical interatomic distance. This asymptot-

ic expression of the induced potential is valid in the harmonic approximation for small enough excitation fields.[17] The prefactor $g(\mathbf{Q},\omega)$ in Eq. (3.2) is the surface dielectric response of the system.[27,28]

For an ionic-crystal film on a thick substrate, lattice dynamics for the semimicroscopic model of Sec. II leads to the following expression of g:

$$g(\mathbf{Q},\omega)=g(\mathbf{Q},\infty)+\sum_j \frac{\rho_j(\mathbf{Q})\omega_j^2(\mathbf{Q})}{\omega_j^2(\mathbf{Q})-\omega^2} , \tag{3.3}$$

where the sum is over all the phonon branches of the film, with dispersion relations $\omega_j(\mathbf{Q})$. The expression for the weight factors $\rho_j(\mathbf{Q})$ valid in a shell-model description can be found in the Appendix, together with the response $g(\mathbf{Q},\infty)$ set up at high frequency by the motion of the zero-mass electronic shells. The formalism can be particularized to rigid ions (see the Appendix). The formulas then simplify in such a way that the following selection rule can be deduced: $\rho_j(\mathbf{Q})$ is zero for those modes linearly polarized parallel to the surface along the direction perpendicular to $\mathbf{Q}$ (SH polarization). The strongest response occurs for optical modes with circular polarization in the sagittal plane.

In a macroscopic picture, the surface dielectric response function of a film with thickness d on a thick substrate is easily derived from elementary electrostatics considerations:[29]

$$g(Q,\omega)=\frac{(\epsilon_1+\epsilon_2)(\epsilon_1-1)-(\epsilon_1-\epsilon_2)(\epsilon_1+1)e^{-2Qd}}{(\epsilon_1+\epsilon_2)(\epsilon_1+1)-(\epsilon_1-\epsilon_2)(\epsilon_1-1)e^{-2Qd}} , \tag{3.4}$$

where $\epsilon_1(\omega)$ and $\epsilon_2(\omega)$ are the bulk dielectric functions of the film and the substrate, respectively. The poles in this expression correspond to the electrostatic eigenmodes of the system, the so-called nonretarded, macroscopic Fuchs-Kliewer (FK) modes.[30] In the context of electrostatics, the long-wavelength FK modes are associated with charge-density oscillations of the form $\sigma e^{i\mathbf{Q}\cdot\rho-i\omega t}$ that develop at both the free surface of the film and the interface with the semi-infinite substrate.[31]

When the overlayer is made from an ionic crystal and for a constant ϵ_2, there are two branches of FK phonons, FK^+ and FK^-, whose dispersion relations $\omega_+(Q)$ and $\omega_-(Q)$ are solutions of $\epsilon_1(\omega_\pm)=-\{\tanh[(Qd\pm X)/2]\}^{\pm 1}$ with $X=\sinh^{-1}[\beta\sinh(Qd)]$, β denoting the screening factor $(\epsilon_2-1)/(\epsilon_2+1)$ introduced previously. Except for $\epsilon_2=1$ (isolated film), the FK^+ and FK^- phonons can be considered as surface and interface modes, respectively. For $Q\neq 0$, the associated charge densities are predominantly localized at the free surface of the film for the former, and at the interface with the substrate for the latter. More precisely stated, a marked surface or interface character stands out when the parameter X introduced above becomes of the order of 1, or larger: the ratio of surface and interface charge densities can indeed be written in the form $\sigma_s/\sigma_i=-e^{+X}$ for FK^+ and $\sigma_s/\sigma_i=+e^{-X}$ for FK^-. For each of these modes, a macroscopic electric field is set up in the vacuum region above the system and the two FK phonons are thus able to respond to an external electric excitation. As ϵ_2 approaches infinity (perfectly conducting substrate), however, only the surface mode can be excited by external sources; its dispersion relation is the same as that of the FK^+ phonon for an isolated film with double thickness.

IV. $CaF_2(111)$ ISOLATED FILMS

Since an isolated film does not demand any of the unknown quantities brought about by the interface with a substrate, this geometry provides us with an ideal situation for testing the validity of the dielectric approximation from lattice-dynamics calculation of the surface response $g(\mathbf{Q},\omega)$. The formalism summarized in the Appendix is directly applicable to any isolated crystalline film by setting $\beta=0$ in the equations. The expression so obtained for the weight factors $\rho_j(\mathbf{Q})$ in Eq. (3.3) reduces to a form close to, although not identical with that of similar oscillator strengths evaluated a long time ago by Evans and Mills for the silicon surface.[6]

In a previous paper,[17] we have already compared the macroscopic and microscopic approaches for g using the rigid-ion approximation. In this section, shell-model calculations are performed for $CaF_2(111)$ isolated films. The shell-model parameters are taken from the literature.[32] The optical constants for the bulk dielectric function $\epsilon_1(\omega)$ of CaF_2 have been deduced from these shell-model parameters, allowing us to test the predictions of the macroscopic approach. Electron-energy-loss spectra are computed from the microscopic theory of $g(\mathbf{Q},\omega)$ and compared with the predictions of the dielectric approximation.[33]

As schematized in Fig. 2, the crystalline structure of an ideal $CaF_2(111)$ film can be viewed as a stacking of CaF_2 layers, each of them consisting of three charged planes with hexagonal arrangements of F, Ca, and F ions, suc-

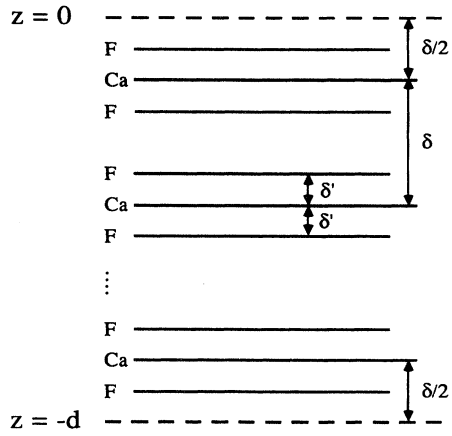

FIG. 2. Crystallographic structure of an ideal $CaF_2(111)$ film. The solid lines represent two-dimensional hexagonal lattices of F or Ca ions. The Ca planes define the usual *ABC* stacking of the face-centered-cubic lattice whose tetrahedral holes are occupied by the F ions. The dashed lines indicate the positions of the geometrical surfaces of the film (see text).

cessively. In the bulk, the spacing δ' between the ionic planes in a layer is one-fourth the interlayer distance δ equal to $a/\sqrt{3}=3.154$ Å in terms of the parameter a of the conventional cubic lattice. For a film composed of N_L CaF_2 layers, the thickness d required by the dielectric approximation [Eq. (3.4)] is defined as $d=N_L\delta$. In other words, the surfaces of the film are geometrical planes located $\delta/2-\delta'=\delta'=0.79$ Å above and below the top and bottom F planes (see Fig. 2). A justification for this can be found in a sum rule satisfied by the oscillator strengths in the expression (3.3) of $g(\mathbf{Q},\omega)$. In the rigid-ion approximation for which an analytical expression of the sum rule can be derived, one finds for the nonrelaxed structure of Fig. 2

$$\sum_j \rho_j(\mathbf{Q})\omega_j^2(\mathbf{Q})=\frac{2}{\pi}\int_0^\infty \mathrm{Im}[g(\mathbf{Q},\omega)]\omega\, d\omega$$
$$=\frac{e^2}{\epsilon_0}\frac{Q}{\Omega}\left[\frac{(2Z)^2}{M_{\mathrm{Ca}}}+2\frac{Z^2}{M_{\mathrm{F}}}\cosh(2Q\delta')\right]\times\frac{1-e^{-2QN_L\delta}}{2\sinh(Q\delta)}\ , \tag{4.1}$$

where Ω is the area of the primitive cell of the film. In this expression, M_{Ca} and M_{F} are the mass of the Ca and F ions, with charges $2Z$ and $-Z$, respectively. For small Q's, Eq. (4.1) reduces to

$$\sum_j \rho_j(\mathbf{Q})\omega_j^2(\mathbf{Q})=\{\omega_I^2+O[(Q\delta)^2]\}\frac{1-e^{-2QN_L\delta}}{2}\ , \tag{4.2}$$

where ω_I is the ionic plasma frequency defined by $\omega_I^2=(e^2/\epsilon_0)[(2Z)^2/M_{\mathrm{Ca}}+2Z^2/M_{\mathrm{F}}]/(\Omega\delta)$.[34] Within the dielectric approximation, on the other hand, Eq. (3.4) with $\epsilon_2=1$ and $\epsilon_1(\omega)=(\omega_{\mathrm{LO}}^2-\omega^2)/(\omega_{\mathrm{TO}}^2-\omega^2)$ compatible with the rigid-ion approximation, yields

$$\frac{2}{\pi}\int_0^\infty \mathrm{Im}[g(\mathbf{Q},\omega)]\omega\, d\omega=(\omega_{\mathrm{LO}}^2-\omega_{\mathrm{TO}}^2)\frac{1-e^{-2Qd}}{2}\ . \tag{4.3}$$

Identifying d with $N_L\delta$ and noticing that $\omega_{\mathrm{LO}}^2-\omega_{\mathrm{TO}}^2=\omega_I^2$ in the present model,[35] Eqs. (4.1) and (4.3) coincide within terms proportional to $(Q\delta)^2$, for an arbitrary number of layers. For deformable ions, the sum rule in the microscopic theory can no longer be expressed in an analytical form. However, we have checked numerically that the first moment of $\mathrm{Im}(g)$ for small wave vectors obtained with the shell model still lies close to its macroscopic counterpart.

We now analyze with some details the results of calculations performed for a $CaF_2(111)$ isolated film composed of $N_L=6$ layers ($d=18.9$ Å). The structure of the film has been relaxed by adjusting the vertical spacings between successive atomic planes so as to minimize the total potential energy of the film. In this simple procedure, there is no core-shell relaxation. It has been found that the static forces computed at the various sites of the relaxed film are virtually zero, in any case considerably smaller than for the nonrelaxed geometry, indicating that indeed the ions are close to equilibrium positions. Relaxations in $CaF_2(111)$ film have been found much larger than for a NaCl(001) structure. The largest modification in the interplane distances is realized between the F plane at a free surface and the next Ca plane, accounting for a reduction of 17% of the bulk value δ'. The value calculated here for $N_L=6$ does not change anymore on increasing the number of layers and is consistent with independent theoretical predictions for (111) surfaces of oxides having the antifluorine structure.[36]

Figure 3 illustrates the dispersion relations of optical phonons close to the center of the surface first Brillouin zone in the CaF_2 relaxed (111) film with $N_L=6$. For selected wave numbers Q, the phonon frequencies $\omega_j(Q)$ of the slab have been represented with dots whose areas are proportional to the relative weight factors $\rho_j(Q)/\sum_{j'}\rho_{j'}(Q)$ in the expression (3.3) of the surface dielectric response. The solid lines are the dispersion curves of the two macroscopic Fuchs-Kliewer (FK) surface phonons deduced from electrostatics for the same system (see Sec. III). As shown in Fig. 3, the weights of the two FK modes of the macroscopic approach are distributed over several branches in the microscopic theory. This implies some interaction between the highly dispersed FK modes and other optical phonons[18,37] which would otherwise present flat dispersion curves in the small domain of wave vectors considered here. The intense phonons around the FK^- and FK^+ curves are linearly polarized normal to the surface ($SP_\perp$) close to $Q=0$. They acquire elliptical polarization in the sagittal plane for larger Q's. Very close to the $\bar{\Gamma}$ point, these phonons present small vibration amplitudes at the surface. By increasing Q, the surface amplitude increases. Away from the FK curves, some phonons still present non-negligible weights in the dielectric response. This is the

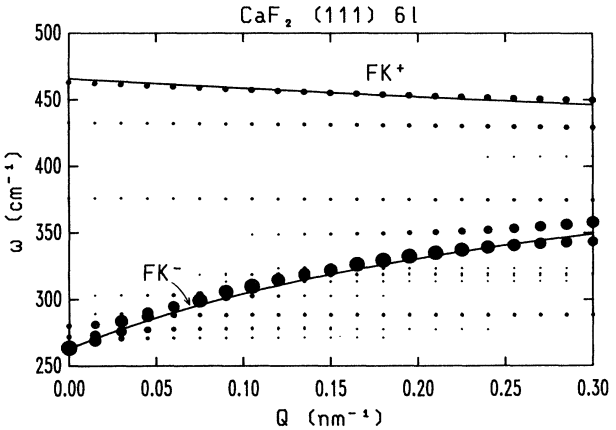

FIG. 3. Optical-phonon dispersion curves (dots) close to the center of the two-dimensional first Brillouin zone for a relaxed $CaF^2(111)$ isolated film composed of six CaF_2 layers (18 atoms per primitive cell). The areas of the dots are proportional to the weight factors $\rho_j(Q)$ in the surface dielectric response of the film [Eq. (3.3)]. Those points with negligible weights have been discarded from the drawing. The solid lines represent the dispersion curves of the two macroscopic surface (FK^- and FK^+) phonons deduced from electrostatics [Eq. (3.4)].

case for a branch with little dispersion around 290 cm^{-1} (Fig. 3) which corresponds to a pair of quasidegenerate transverse-optical surface microscopic phonons, with predominant $SP_{\perp}$ polarization. For the 6-layer CaF_2 relaxed film, as well as for an 11-layer slab where this branch is still observed at nearly the same frequency, the related eigenvectors are found to be larger at the first surface layer and rapidly decreasing as the distance from the surface increases; in the first surface layer, the F atoms on both sides of the Ca plane (Fig. 2) vibrate against each other with an amplitude much larger than that of the Ca ions.

Figure 4 shows EELS spectra computed for the isolated film of Fig. 3, using either the macroscopic expression of g (solid curve) or the microscopic one (dotted curve). These theoretical spectra have been convoluted with a hypothetical instrumental broadening function whose width (30 cm^{-1}) is typical of the energy resolution achieved in today's EELS experiments. Hence, because of realistic instrumental limitations that were simulated in the calculations, the differences between the dispersions relations illustrated in Fig. 3 for this CaF_2 thin film do not manifest themselves in the EELS spectrum, the two curves of Fig. 4 being hardly distinguishable from each other. The FK^- mode is responsible for the intense loss and gain peaks around 300 cm^{-1} on both sides of the elastic peak at zero frequency. The peak with smaller amplitude around 450 cm^{-1} is the signature of the FK^+ mode. The structure observed at higher frequencies represents multiple-scattering events: emission by the probing electrons of two FK^- phonons (600 cm^{-1}), or a combination of FK^- and FK^+ (750 cm^{-1}). The small peak visible in the amplified part of the spectrum at 150 cm^{-1} in the gain region is the consequence of successive absorption and emission of FK^- and FK^+ phonons.

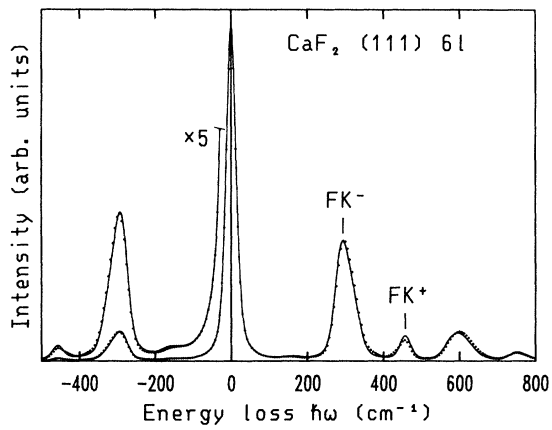

FIG. 4. The EELS spectrum of a relaxed $CaF_2(111)$ isolated film with $N_L = 6$ layers has been computed at room temperature for 6.1-eV electrons specularly reflected at the surface under an incidence of 45°, using either the macroscopic theory of $g(\mathbf{Q},\omega)$ (solid curve) or the microscopic one (dotted curve). The spectra have been broadened by convolution product with a typical instrumental width [full width at half maximum (FWHM) = 30 cm^{-1}].

Using similar data, the positions of single-loss peaks attributed to the FK^- and FK^+ modes were traced on the computed EELS spectra for various numbers N_L of layers in $CaF_2(111)$ isolated films, using both the macroscopic and the microscopic approaches. The results are displayed in Fig. 5. In the lattice-dynamics calculations, the effects of surface relaxation have been investigated. As shown in Fig. 5, relaxing the structure has little effect on the position of FK^+. By contrast, the frequency of FK^- lies below or above the position predicted by electrostatics for the nonrelaxed or relaxed lattices, respectively. This is due to a strong interaction at $Q=0$ between the FK^- mode and the surface microscopic S_4^+ phonon[38] whose frequency shifts upwards and enters the TO bulk band when relaxing the structure. This interaction is particularly important for very thin films. With more than ten CaF_2 layers, the EELS spectra computed for both the relaxed and unrelaxed structures become indistinguishable from each other. If the macroscopic theory does not succeed in producing the results of the microscopic approach for very thin films ($N_L \leq 4$), the discrepancies between the models gradually decrease for larger thickness. The thickness dependence of the dotted curves (relaxed films) in Fig. 6 agrees qualitatively well with experimental EELS data available for $CaF_2(111)$

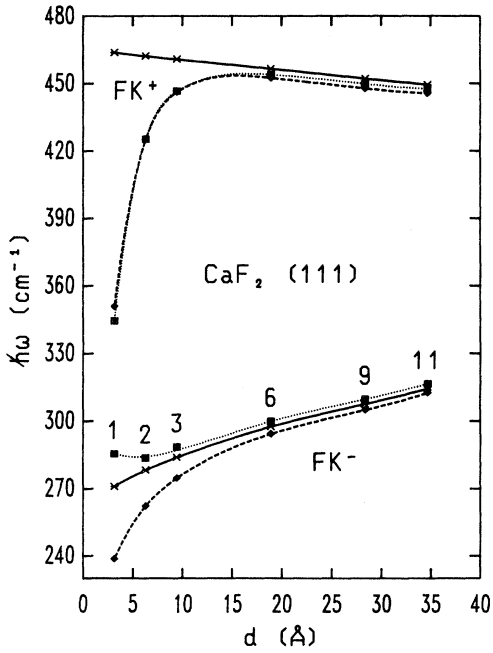

FIG. 5. Position of the single-loss peaks attributed to the two macroscopic FK^- (bottom) and FK^+ (top) phonons as traced from computed EELS spectra similar to the one of Fig. 4 for CaF_2 (111) isolated films. The curves are guides for the eyes, which interpolate the data obtained for films composed of N_L = 1, 2, 3, 6, 9, and 11 CaF_2 layers. The surface dielectric response function has been obtained either from the macroscopic approach (solid curve) or the microscopic theory for both nonrelaxed (dashed curve) or relaxed (dotted curve) films.

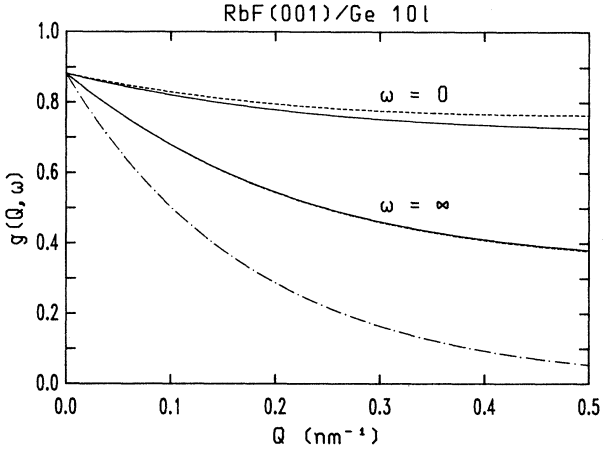

FIG. 6. Static ($\omega=0$) and high-frequency ($\omega=\infty$) surface dielectric response function $g(Q,\omega)$ of a ten-layer RbF(001) relaxed film onto a dielectric Ge substrate as obtained from electrostatics (solid curves) or lattice-dynamical calculations within the semimicroscopic model described in Sec. II (dashed curves). The two curves for $\omega=\infty$ are hardly distinguishable at the scale of the drawing. The dot-dashed curve shows the dielectric response βe^{-2Qd} of the Ge dielectric substrate alone (see the Appendix).

films on Si,[20] although the deviation of the experimental points with respect to the electrostatics predictions are larger than what we find theoretically for self-supported films. With more than six CaF_2 layers in the present calculations, there is no appreciable difference in both the position and the intensity of the peaks in the EELS spectra deduced from the microscopic or the macroscopic theories of the surface dielectric response.

V. RbF(001)/Ge

We now turn our attention to an overlayer geometry by considering the case of RbF(001) films on a thick Ge substrate, a system that can actually be made epitaxic[39] and for which the concepts developed in Sec. II apply directly. Lattice-dynamical calculations for RbF are based on a shell model.[40] Assuming central forces for the anion-cation repulsive interactions, we have adjusted the second-neighbor cation-cation and anion-anion transverse force constants B_{++} and B_{--} by identifying them through the equilibrium condition of the bulk lattice,[26]

$$\tfrac{2}{3}\alpha_M Z^2+B_{+-}+2(B_{++}+B_{--})=0\ , \qquad (5.1)$$

where α_M is the bulk Madelung constant and β_{+-} is the nearest-neighbor cation-anion transverse force constant. This procedure does not affect the long-wavelength bulk dielectric properties of the crystal and enables us to relax the films. Still neglecting core-shell relaxations, the structural relaxations were found to be small in RbF(001)/Ge, as already suggested by Eq. (2.3) and the discussion that immediately follows.

The surface dielectric response of RbF(001) relaxed films has been computed for short wave vectors and compared with the predictions of electrostatics using $\epsilon_2=16$ for the dielectric constant of the Ge substrate. The thickness of a film composed of N_L atomic planes is here again defined as $d=N_L\delta$,[17] with δ the interlayer spacing (see Fig. 1). As an example of comparison between the (semi)microscopic and macroscopic approaches, Fig. 6 represents the static and high-frequency response functions $g(\mathbf{Q},0)$ and $g(\mathbf{Q},\infty)$ versus the wave number Q for a ten-layer film ($d=28$ Å). In both macroscopic and microscopic models, $g(0,\omega)=\beta$ for $Q=0$ (see the Appendix), irrespective of ω, where $\beta=\frac{15}{17}$ is the image screening factor of the Ge substrate. It immediately appears from Fig. 6 that lattice-dynamical determination of the high-frequency response of the present system is nicely reproduced by the much simpler dielectric approximation. For the static response and for the small wave vectors predominantly probed in specular EELS ($Q\approx 0.1$ nm^{-1}), the deviation observed between the two approaches, although small, is significant. Remark that $g(\mathbf{Q},\infty)$ does not influence the computation of the EELS spectra that only demands the imaginary part of the surface dielectric response. By contrast, the difference $g(\mathbf{Q},0)-g(\mathbf{Q},\infty)$, being related to the total loss intensity, is an important quantity. As discussed below, the difference between the two determinations of $g(\mathbf{Q},0)-g(\mathbf{Q},\infty)$ is mainly the consequence of the response of surface microscopic RbF phonons that electrostatics is unable to account for.

Figure 7 shows dispersion relations of optical phonons in RbF(001)/Ge with $N_L=10$ using the same representation as in Fig. 3. The solid curves are the electrostatics Fuchs-Kliewer modes. For increasing wave numbers Q, FK^+ and FK^- acquire more and more pronounced surface and interface characters, respectively, as explained in Sec. III. In contrast with the case of an isolated film, most of the spectral weight is now distributed around the

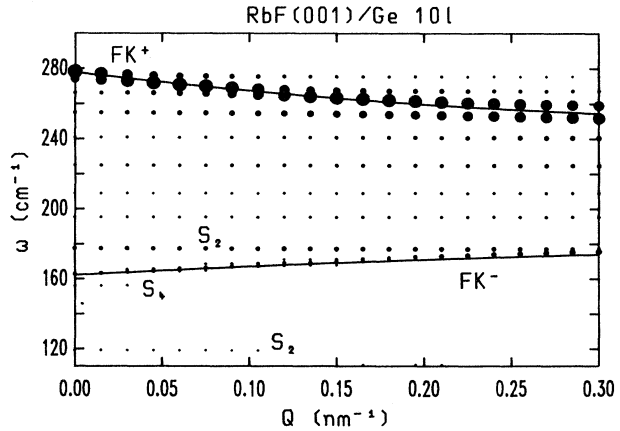

FIG. 7. Same representation as in Fig. 3 of optical-phonon branches around the $\bar{\Gamma}$ point for RbF(001)/Ge with $N_L=10$. The dispersion curves of the two Fuchs-Kliewer modes of the macroscopic approach are represented by solid lines. The structure of the film has been relaxed for the semimicroscopic lattice-dynamics calculations of the surface dielectric response (dots).

FK^+ (surface) mode. The intense phonons in this region have elliptical polarization in the sagittal plane with dominant $SP_\perp$ character, as previously. The phonons having the highest response around FK^- are also polarized in the sagittal plane but this time with a dominant $SP_\parallel$ character. The corresponding eigenvectors are found to have small amplitudes at the interface or at the free surface close to $Q=0$. On increasing Q, there remain appreciable amplitudes in the interior of the film; the interface components of the eigenvectors increase with respect to the surface components, however, conferring to these phonons a macroscopic interface character in complete agreement with electrostatic predictions.

As for the case of isolated films, several microscopic phonons participate in the surface dielectric response. The branch with little dispersion just below 180 cm^{-1} in Fig. 7 is an S_2 surface microscopic phonon localized at the free surface of the RbF(001) film. In a self-supported film, there would be two such phonons, $S_2^\pm$ with even and odd parities with respect to the symmetry plane at half thickness and nearly degenerate frequencies at about 177 cm^{-1}.[38] With the Ge substrate, the symmetry is broken and the $S_2^\pm$ pair splits into two modes predominantly localized either at the surface or at the interface. The upper S_2 mode in Fig. 7 is the surface phonon whose frequency is only weakly affected by the substrate. Its weight at small Q's is of the same magnitude as, or larger than, that of the FK^- macroscopic mode (see Fig. 7).

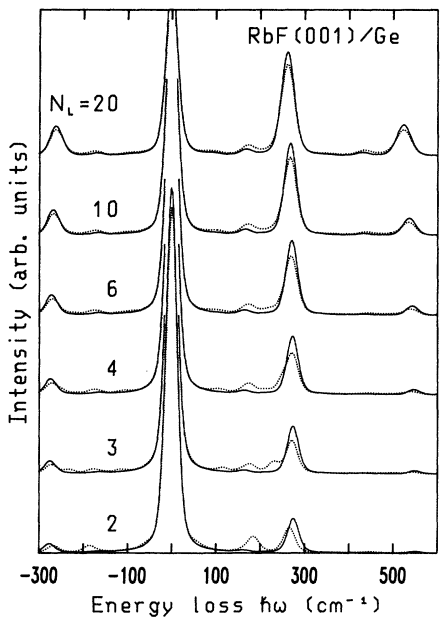

FIG. 8. Theoretical EELS spectra of RbF(001)/Ge deduced from the macroscopic theory (solid curves) or the semimicroscopic lattice-dynamics calculations (dotted curves) of the surface dielectric function for relaxed films composed of 2, 3, 4, 6, 10, and 20 layers. The electron kinetic energy and incidence angle are 5 eV and 45°, respectively. The spectra have been convoluted with a typical instrumental broadening function (30-cm^{-1} resolution).

The lower S_2 microscopic phonon found at 119 cm^{-1} is the interface mode. Similarly, the branch around 156 cm^{-1} with little response close to the $\bar{\Gamma}$ point is an S_4 surface microscopic mode;[38] its interface partner has a negligible weight in the surface dielectric response. It is worth remembering that interface microscopic phonons are only approximately reproduced by the present calculations due to the continuous-medium approximation used in treating the substrate. In fact, the dielectric response set up by these modes is weak, as it can be inferred from the weights representing the S_2 interface phonons in Fig. 7. So $g(\mathbf{Q},\omega)$, being mostly dominated by the FK^+ mode and to a lesser extent by other surface optical phonons, should essentially be correct.

EELS room-temperature spectra have been computed for RbF(001) films on Ge from both the microscopic and macroscopic determinations of $g(\mathbf{Q},\omega)$. The results are shown in Fig. 8. For very thin films, the FK^- loss peaks are hardly visible when using the dielectric theory (solid curves). With the semimicroscopic approach (dotted curves), by contrast, a two- or three-peak structure is clearly resolved within the 150–300-cm^{-1} single-loss range for $N_L=2$ or 3, respectively. For a larger thickness, phonons in the FK^- regions (160–180 cm^{-1}) contribute to the spectrum in the form of a weak structure in the low-frequency wing of the dominant FK^+ peak whose intensity grows as N_L increases. With ten layers or more, the *positions* of the loss peaks determined by the microscopic and macroscopic approaches agree quite well. Discrepancies remain between the loss *intensities*, even when $N_L=20$ ($d=56$ Å). The deviation between the two EELS spectra for the 20-layer RbF film is nevertheless small on the absolute scale, even if the intensity of the FK^- loss peak predicted by the dielectric theory is roughly one-half the one obtained from the semimicroscopic model. This discrepancy chiefly results from the non-negligible response of the S_2 surface microscopic phonon, as explained above.

VI. DISCUSSION

The calculations presented in this paper were aimed at investigating the effects of the thickness in the application of the dielectric approximation for determining the long-wavelength surface dielectric function of a thin film. The semimicroscopic model of Sec. II, by eliminating all the microscopic details about the interface, was designed for that purpose. It appears from Figs. 5 and 8 that films composed of less than (say) five "molecular" layers are definitively below the applicability domain of electrostatics. Even for thicker films, obvious characteristics of the optical-phonon structure are missing in the macroscopic determination of $g(\mathbf{Q},\omega)$, at least in that the Fuchs-Kliewer macroscopic modes hybridize with several phonons in the lattice dynamics (Figs. 3 and 7). Detecting such effects is, however, crucially dependent upon the frequency resolution of the spectrometer used to analyze the response to long-wavelength excitations. Nevertheless, the EELS spectra calculated for RbF(001) /Ge clearly indicate a contribution of the S_2 microscopic phonon localized at the free surface of RbF: for a 20-layer film, this

phonon participates for half the intensity of the loss peak in the region of the FK^- mode.

Such a signature of a surface microscopic phonon should not be specific to the particular RbF(001)/Ge system. It is believed that a similar situation might be realized for $CaF_2(111)$ overlayers. Figure 3, which is for an isolated film, clearly indicates a nonvanishing dielectric response of the transverse-optical surface microscopic phonon at 290 cm^{-1}. The contribution of this mode (in fact, a pair of quasidegenerate microscopic S_2 modes) to the EELS spectrum is hidden by the intense FK^- phonon (Fig. 4). This would no longer be true with a Si substrate, due to the dramatic screening the substrate would produce on the weight of the FK^- mode. Besides, the presence of the substrate should not affect strongly the frequency of the surface partner of this pair of microscopic phonons when $N_L \gtrsim 6$ (as indeed observed for the RbF/Ge system) and the contribution of this surface microscopic phonon to the EELS spectrum of CaF_2/Si might now well become comparable to that predicted for the FK^- macroscopic mode (as it was indeed the case in Figs. 7 and 8). In connection with this discussion, it is interesting to mention that the frequency of the FK^- peak in the experimental loss spectra of CaF_2Si(111) shows little dispersion, precisely around 290 cm^{-1}, when plotted against the overlayer thickness in the 10–50-Å range.[20] By contrast, EELS calculations performed within the dielectric approximation predict a monotonous shift of the FK^- loss peak from 265 ($d=10$ Å) to 285 cm^{-1} ($d=50$ Å). A possible explanation of the experimental EELS observations is therefore that for thin overlayers, the optical-transverse microscopic phonon localized at the free surface of $CaF_2(111)$ contributes substantially to the loss structure found around 290 cm^{-1}, which can no longer be attributed solely to the "interface" FK^- mode. The fact that the intensity of the loss peak in this region is about twice that predicted by the dielectric theory, as found in recent experimental EELS measurements on CaF_2/Si(111),[41] corroborates the above interpretation.

Apart from such relatively small effects, one can conclude from Figs. 4 and 8 that the dielectric approximation works reasonably well for films made of ionic crystals of more than 6–10 layers: with the limited energy-loss resolution in specular EELS, a bulk dielectric function makes sense when applied to overlayers whose thickness exceeds 20–30 Å. For thicker continuous films, failure of the dielectric theory in reproducing at least the positions of the phonon loss peaks in experimental EELS data should not question the applicability of electrostatics concepts. This would rather indicate that the structure of the film differs from that of the bulk to such an extent that the dielectric function of the bulk crystal is no longer representative of the material in its layered form. Such an explanation has indeed been invoked to explain the observed failure of the dielectric approximation in describing EELS spectra of CaF_2 layers on Si(111) for thickness above 100 Å, the argument being that the lattice mismatch between fluorine and silicon at growth temperature introduces strains that can affect the dielectric function.[20]

ACKNOWLEDGMENTS

This work was funded by the Interuniversity Research Project (PAI) on Interface Sciences initiated by the Belgian State Prime Minister's Office (Science Policy Programming). Ph.L. acknowledges the Belgian National Fund for Scientific Research (FNRS). P.S. is grateful to the "Institut pour l'Encouragement de la Recherche Scientifique dans l'Industrie et l'Agriculture (IRSIA)" for financial support. The authors acknowledge the use of the Namur Scientific Computing Facility, a common project between the FNRS, IBM-Belgium, and the FUNDP.

APPENDIX

We consider a film with n ions per primitive cell of the surface Bravais lattice on a thick dielectric substrate with dielectric constant ϵ_2. The free surface of the film is defined as the $z=0$ plane and the interface with the substrate is located at $z=-d$. In the presence of an external potential ϕ_e of the form given by Eq. (3.1), the potential ϕ_a actually applied to an ion at location $\mathbf{r}=\rho+z\hat{\mathbf{e}}_z$ in the film is the sum of ϕ_e plus the potential induced by the substrate:[17]

$$\phi_a(\mathbf{r},t)=A(1-\beta e^{-2Q(z+d)})e^{Qz}e^{i\mathbf{Q}\cdot\rho-i\omega t}, \quad -d<z<0, \tag{A1}$$

where $\beta=(\epsilon_2-1)/(\epsilon_2+1)$ is the screening factor introduced previously. The electric field applied to an ion labeled κ at its equilibrium position $\tau(\kappa)$ in the primitive cell at the origin is, therefore,

$$\mathbf{E}_a(\kappa,t)=-iA(\gamma-\beta e^{-2Q[\tau_z(\kappa)+d]}\gamma^*)\times e^{i\gamma\cdot\tau(\kappa)-i\omega t}, \tag{A2}$$

where we have introduced the three-dimensional complex wave vector $\gamma=\mathbf{Q}-iQ\hat{\mathbf{e}}_z$, Q being the modulus of the surface wave vector $\mathbf{Q}$, and γ^* denotes the complex conjugate of γ. In the harmonic approximation, the electric field $\mathbf{E}_a$ is responsible for plane-wave oscillations of the ions around their equilibrium positions, which in turn induce a response potential whose asymptotic expression at a large distance from the free surface of the film will now be evaluated.

We first consider the response to a high-frequency field in order to illustrate how the formalism works, the present situation being simpler than that encountered for a finite frequency. In a standard shell-model description, the ion κ in a primitive cell is composed of a massless, spherical electronic shell that carries a charge Y_κ in units of e, harmonically bound to its core with mass M_κ and charge X_κ. As ω approaches infinity, the ionic cores stay at rest at their equilibrium positions whereas the zero-mass electronic shells follow instantaneously the excitation force. The displacement of the shells are plane waves of the form $\mathbf{w}(\kappa,t)e^{i\mathbf{Q}\cdot\mathbf{T}}$, with an amplitude $\mathbf{w}(\kappa,t)$ that represents the displacement of the shell κ in the unit cell at the origin and where $\mathbf{T}$ denotes a two-dimensional Bravais translation. The electrical response of the film to

the high-frequency limit of the potential (A1) is defined as the difference between the potential set up by the vibrating shells and the Coulomb potential of the shells at rest, to which we add the corresponding contributions arising from the images across a mirror plane at $z=-d$. Accordingly, the response potential at location $\mathbf{r}$ above the film, developed to first order in the assumed-small displacements, is written as

$$\phi_{\rm res}(\mathbf{r},t)=-\frac{e}{4\pi\epsilon_0}\nabla_{\mathbf{r}}\cdot\sum_{\kappa=1}^{n}\left[Y_\kappa\mathbf{w}(\kappa,t)\sum_{\mathbf{T}}\frac{e^{i\mathbf{Q}\cdot\mathbf{T}}}{|\mathbf{r}-\boldsymbol{\tau}(\kappa)-\mathbf{T}|}-\beta Y_\kappa\mathcal{J}\mathbf{w}(\kappa,t)\sum_{\mathbf{T}}\frac{e^{i\mathbf{Q}\cdot\mathbf{T}}}{|\mathbf{r}-\hat{\boldsymbol{\tau}}(\kappa)-\mathbf{T}|}\right], \tag{A3}$$

where $\mathcal{J}$ is the imaging matrix [Eq. (2.4)] and $\boldsymbol{\tau}_{\hat{\jmath}}(\kappa)$ denotes the image of the equilibrium position of the shell attached to the site κ. The response potential (A3) is not the full potential induced by the complete system composed of the film and the dielectric substrate; we still have to add the response of the substrate to the external potential (3.1). The latter being the term proportional to β in Eq. (A1), the complete expression of the induced potential is written as

$$\phi_{\rm ind}(\mathbf{r},t)=\phi_{\rm res}(\mathbf{r},t)-\beta Ae^{-Q(2d+z)}e^{i\mathbf{Q}\cdot\boldsymbol{\rho}-i\omega t}\ .$$

In this expression, as in Eqs. (A3)–(A6), β is the high-frequency surface screening factor of the substrate; with our assumption of an ω-independent dielectric constant ϵ_2, the substrate response does not depend on ω and its contribution is incorporated into the high-frequency limit of $g(\mathbf{Q},\omega)$. This is so because $g(\mathbf{Q},\infty)$ is an additive constant in the frequency-dependent part of the surface dielectric function (3.3).

As usual, the lattice sums in Eq. (A3) are best performed in Fourier space using Poisson's formula. The expressions so obtained involve summations over all the two-dimensional reciprocal vectors $\mathbf{G}$. However, as the distance z above the surface increases, the sums in the reciprocal lattice are dominated by the sole $\mathbf{G}=\mathbf{0}$ terms defining the macroscopic potential. After little algebraic manipulations, the induced potential so obtained takes the following asymptotic expression as $z\to\infty$:

$$\phi_{\rm ind}(\mathbf{r},t)=-i\frac{2\pi}{\Omega Q}\frac{e}{4\pi\epsilon_0}\sum_{\kappa=1}^{n}Y_\kappa e^{-i\boldsymbol{\gamma}^*\cdot\boldsymbol{\tau}(\kappa)}(\boldsymbol{\gamma}^*-\beta e^{-2Q[\tau_z(\kappa)+d]}\boldsymbol{\gamma})\cdot\mathbf{w}(\kappa,t)e^{i\mathbf{Q}\cdot\boldsymbol{\rho}}e^{-Qz}-\beta Ae^{-Q(2d+z)}e^{i\mathbf{Q}\cdot\boldsymbol{\rho}-i\omega t}\ , \tag{A4}$$

where Ω is the area of the surface primitive cell.

Equation (A4) still demands the shell displacements $\mathbf{w}$. These can be obtained by solving the equations of motion for the zero-mass shells, the high-frequency limit of which simplifies into

$$\sum_{\kappa'=1}^{n}\Phi^{\rm dd}(\kappa,\kappa';\mathbf{Q})\mathbf{w}(\kappa',t)=eY_\kappa\mathbf{E}_a(\kappa,t)\ ,\quad \kappa=1,2,\ldots,n\ , \tag{A5}$$

where the right-hand side represents the driving force set up by the applied field [Eq. (A2)], whereas the left-hand side is the restoring force acting on the shell at site κ as the result of plane-wave displacements of all the shells. The so-called dipole-dipole force constants Φ^{dd} are 3×3 symmetric tensors representing Bloch sums of the force constants associated with all the shell-shell interaction potentials, including the substrate contribution through the images of the shells, as stated by Eq. (2.7). The elements $\Phi^{dd}(\kappa,\kappa;\mathbf{Q})$ for $\kappa'=\kappa$ also incorporate the force constants of the interaction that binds the shell κ to its core.[42]

Solving the sets of equations (A5) for the shell displacements requires inverting the $3n\times3n$ dipole-dipole matrix. Applying the inverse dipole-dipole matrix on the left of Eq. (A5) allows us to express the displacements as linear combinations of the driving forces acting on the various shells. These forces, through the expression (A2) of the applied field, are proportional to the amplitude A of the external potential [Eq. (3.1)]. Inserting the developments so obtained for $\mathbf{w}(\kappa,t)$ into the left-hand side of Eq. (A4) leads to an expression that can be identified with Eq. (3.2). This identification yields the following formula for the high-frequency surface dielectric response:

$$g(\mathbf{Q},\infty)=\beta e^{-2Qd}+\frac{e^2}{\epsilon_0}\frac{Q}{\Omega}\sum_{\kappa,\kappa'}Y_\kappa e^{-i\boldsymbol{\gamma}^*\cdot\boldsymbol{\tau}(\kappa)}(\hat{\boldsymbol{\gamma}}^*-\beta e^{-2Q[\tau_z(\kappa)+d]}\hat{\boldsymbol{\gamma}})\cdot D(\kappa,\kappa';\mathbf{Q})\cdot(\hat{\boldsymbol{\gamma}}-\beta e^{-2Q[\tau_z(\kappa')+d]}\hat{\boldsymbol{\gamma}}^*)e^{i\boldsymbol{\gamma}\cdot\boldsymbol{\tau}(\kappa')}Y_{\kappa'}\ , \tag{A6}$$

where $\hat{\boldsymbol{\gamma}}=\boldsymbol{\gamma}/\sqrt{2}Q$ is the normalized three-dimensional complex wave vector introduced above. In Eq. (A6), the n^2 matrices $D(\kappa,\kappa';\mathbf{Q})$ stand for 3×3 blocks of the inverse dipole-dipole matrix, i.e., their Cartesian components $D_{\alpha,\alpha'}$ are solutions of the set of equations

$$\sum_{\kappa'',\alpha''}\Phi^{dd}_{\alpha\alpha''}(\kappa,\kappa'';\mathbf{Q})D_{\alpha''\alpha'}(\kappa'',\kappa';\mathbf{Q})=\delta_{\kappa,\kappa'}\delta_{\alpha,\alpha'}\ . \tag{A7}$$

For finite frequencies, we have to include the contributions of the cores and their images. The derivation of the

frequency-dependent part of the surface dielectric response $g(\mathbf{Q},\omega)$ for an isolated film has been the subject of a previous work. How to account for the presence of a dielectric substrate is a straightforward extension of that work which will be detailed here. The expression of $g(\mathbf{Q},\omega)$ obtained is that given by Eq. (3.3), with resonances at the $3n$ eigenfrequencies $\omega_j(\mathbf{Q})$ of the slab and oscillator strengths

$$\rho_j(\mathbf{Q})\omega_j^2(\mathbf{Q})=\frac{e^2}{\epsilon_0}\frac{Q}{\Omega}\left|\sum_{\kappa=1}^{n}\frac{e^{i\gamma\cdot\tau(\kappa)}}{\sqrt{M_\kappa}}\mathbf{e}_j^*(\kappa;\mathbf{Q})\cdot[Z(\kappa;\mathbf{Q})\hat{\gamma}-\beta e^{-2Q[\tau_z(\kappa)+d]}Z'(\kappa;\mathbf{Q})\hat{\gamma}^*]\right|^2 . \tag{A8}$$

In this equation, $\mathbf{e}_j(\kappa;\mathbf{Q})$ is the polarization vector (projection of the jth eigenvector of the dynamical matrix on the side κ) associated with the jth phonon branch; $Z(\kappa;\mathbf{Q})$ and $Z'(\kappa;\mathbf{Q})$ are 3×3 tensors that represent apparent charges of the ion κ and its image, respectively. For nondeformable ions, both of them reduce to $Z_\kappa E$, with E the 3×3 unit tensor and where $Z_\kappa=X_\kappa+Y_\kappa$ is the net charge of ion κ. Equation (A8) then reproduces an expression we have already derived for rigid ions.[17] The apparent charges for deformable ions and their images in the present slab geometry are defined by

$$Z(\kappa;\mathbf{Q})=Z_\kappa E-\sum_{\kappa',\kappa''}\Phi^{\mathrm{ad}}(\kappa,\kappa';\mathbf{Q})D(\kappa',\kappa'';\mathbf{Q})Y_{\kappa''}\times e^{i\gamma\cdot[\tau(\kappa'')-\tau(\kappa)]} , \tag{A9}$$

$$Z'(\kappa;\mathbf{Q})=Z_\kappa E-\sum_{\kappa',\kappa'}\Phi^{\mathrm{ad}}(\kappa,\kappa';\mathbf{Q})D(\kappa',\kappa'';\mathbf{Q})Y_{\kappa''}\times e^{i\gamma^*\cdot[\tau(\kappa'')-\tau(\kappa)]} . \tag{A9'}$$

In these expressions, the D's are the matrices defined in Eq. (A7) and ϕ^{ad} is the analog of ϕ^{dd} for the so-called atom-dipole force constants, incorporating the core-shell and shell-shell interactions[42] and including the image contributions. The expressions (A9) and (A9') of the apparent charges differ from their form usually found in the literature[42] by the presence of the phase factors $e^{i\cdots}$ which explicitly account for the spatial variation of the applied electric field (A2). At the $\bar{\Gamma}$ point these phase factors disappear, the two expressions (A9) and (A9') coincide and reproduce the usual definition of the apparent charge.

For an isolated film ($\beta=0$) having the NaCl(001) structure, the apparent charge $Z(\kappa,0)$ for $Q=0$ is a diagonal tensor with identical components along two directions parallel to the surface and equal to the transverse (Born) effective charge Z_T^* of the ion κ, whereas the normal component of the tensor is identified with the longitudinal (Collen) effective charge Z_L^*. This is true for sites κ in the interior of a reasonably thick film ($N_L \gtrsim 8$). (Such a uniaxial form of the apparent charge has already been assumed in Ref. 6.) It is worth noticing that $Z(\kappa,0)$ for an ion κ at or close to the surface differs from the expression we give for the central part of the film. Moreover, the latter does coincide with the long-wavelength apparent charge Z_T^*E of the three-dimensional crystal[42] when the thickness of the film is allowed to approach infinity. This is as a consequence of the macroscopic depolarization field of the slab.

[1]See, e.g, S. Luryi, in *Physics, Fabrication and Applications of Multilayered Structure,* Vol. 182 of *NATO Advanced Study Institute, Series B: Physics,* edited by P. Dhez and C. Weisbuch (Plenum, New York, 1988), pp. 241–270.

[2]For a recent review, see P. Masri, Surf. Sci. Rep. **9**, 295 (1988).

[3]A. A. Lucas, J.-P. Vigneron, Ph. Lambin, P. A. Thiry, J.-J. Pireaux, and R. Caudano, Phys. Scr. T **13**, 150 (1986).

[4]D. L. Mills, Surf. Sci. **158**, 411 (1985).

[5]A. A. Lucas and M. Sunjic, Phys. Rev. Lett. **26**, 229 (1971).

[6]E. Evans and D. L. Mills, Phys. Rev. B **5**, 4126 (1972).

[7]B. N. J. Persson and J. E. Demuth, Phys. Rev. B **30**, 5968 (1985).

[8]J. F. Annett, R. E. Palmer, and R. F. Willis, Phys. Rev. B **37**, 2408 (1988).

[9]W. Schaich, Surf. Sci. **122**, 175 (1982).

[10]Ph. Lambin, J.-P. Vigneron, and A. A. Lucas, Phys. Rev. B **32**, 8203 (1985).

[11]A. G. Eguiluz and D. A. Campbell, Phys. Rev. B **31**, 7572 (1985).

[12]A. Liebsch, Phys. Scr. **35**, 354 (1987).

[13]A. G. Eguiluz, Phys. Scr. **36**, 651 (1987), and references therein.

[14]For a recent application of this approach to the Si(111)-2×1 reconstructed surface, see F. Ancilotto, W. Andreoni, A. Selloni, R. Car, and M. Parrinello, Phys. Rev. Lett. **65**, 3148 (1990).

[15]R. M. Martin and K. Kunc, Phys. Rev. B **24**, 2081 (1981).

[16]P. Giannozzi, S. de Gironcoli, and R. Resta, in *Proceedings of the 3rd International Conference on Phonon Physics, Heidelberg, 1989,* edited by S. Hunglinger, W. Ludwig, and G. Weiss (World Scientific, Singapore, 1990), p. 205.

[17]P. Senet, Ph. Lambin, J.-P. Vigneron, I. Derycke, and A. A. Lucas, Surf. Sci **226**, 307 (1990).

[18]W. E. Jones and R. Fuchs, Phys. Rev. B **4**, 3581 (1971).

[19]B. G. Dick, Jr. and A. W Overhauser, Phys. Rev. **112**, 90 (1958).

[20]M. Liehr, P. A. Thiry, J. -J. Pireaux, and R. Caudano, Phys. Rev. B **34**, 7471 (1986).

[21]G. Benedek, Surf. Sci. **61**, 603 (1976); G. Benedek, Physicallia Mag. Suppl. **7**, 3 (1985).

[22]B. N. J. Persson, Solid State Commun. **24**, 573 (1977).

[23]M. Sunjic, R. Brako, Z. Lenac, and D. Sokcevic, Int. J. Quantum Chem. **12**, Suppl. 2, 59 (1977).

[24]L. J. Schowalter and R. W. Fathauer, J. Vac. Sci. Technol. A **4**, 1026 (1986).

[25]R. A. Cowley, W. Cochran, B. N. Brockouse, and A. D. B. Woods, Phys. Rev. **131**, 1030 (1963).

[26]F. W. de Wette, W. Kress, and U. Schröder, Phys. Rev. B **32**, 4143 (1985).

[27]P. J. Feibelman, Prog. Surf. Sci. **12**, 287 (1982).

[28]B. N. J. Persson and E. Zaremba, Phys. Rev. B **31**, 1863 (1985).
[29]H. Froitzheim, H. Ibach, and D. L. Mills, Phys. Rev. B **11**, 4980 (1975).
[30]R. Fuchs and K. L. Kliewer, Phys. Rev. **140**, A2076 (1965).
[31]K. L. Kliewer and R. Fuchs, Adv. Chem. Phys. **27**, 355 (1974).
[32]Two independent parameter sets have been proposed by M. M. Elcombe and A. W. Pryor, J. Phys. C **3**, 492 (1970). After correction for an obvious typographical error, as reported by D. M. Poke and S. D. Devine, J. Phys. C **17**, 3531 (1984), the surface dielectric responses deduced from the two parameter sets were found in close agreement.
[33]See Ph. Lambin, J.-P. Vigneron, and A. A. Lucas, Comput. Phys. Commun. **60**, 351 (1990) for computational details.
[34]M. F. Thorpe and S. W. de Leeuw, Phys. Rev. B **33**, 8490 (1986).
[35]J. D. Axe, Phys. Rev. **139**, A1215 (1965).
[36]W. C. Mackrodt, Phys. Chem. Minerals **15**, 228 (1988).
[37]A. A. Maradudin, R. F. Wallis, and L. Dobrzinski, *Handbook of Surfaces and Interfaces* (Garland STPM, New York, 1980), Vol. 3.
[38]T. S. Chen, F. W. de Wette and G. P. Alldredge, Phys. Rev. B **15**, 1167 (1977).
[39]B. Konrad, C. A. Schug, and W. Steinmann, Surf. Sci. **213**, 412 (1989).
[40]The parameters are those defining the model II in G. Raunio and S. Rolandson, Phys. Rev. B **2**, 2098 (1970); **6**, 2511(E) (1972).
[41]J.-L. Longueville and P. A. Thiry (unpublished).
[42]G. Venkataraman, L. A. Feldkamp, and V. C. Sahni, *Dynamics of Perfect Crystals* (MIT Press, Cambridge, MA, 1975).